Modeling mixed columnar-equiaxed solidification of Sn-10wt%Pb alloy under forced convection driven by travelling magnetic stirring

IOP Conf. Series: Materials Science and Engineering **861** (2020) 012024 doi:10.1088/1757-899X/861/1/012024

Modeling mixed columnar-equiaxed solidification of Sn-10wt%Pb alloy under forced convection driven by travelling magnetic stirring

Z Zhang, M Wu, H Zhang, E Karimi-Sibaki, A Ludwig and A Kharicha

Chair of Simulation and Modelling of Metallurgical Processes, Department of Metallurgy, Montanuniversitaet Leoben, A-8700 Leoben, Austria.

E-mail: menghuai.wu@unileoben.ac.at

Abstract: A mixed columnar-equiaxed solidification model was used to investigate the solidification benchmark experiments, as performed at SIMAP Laboratory. The first experiment case of the benchmark made under natural convection condition was successfully simulated previously. The current work is to simulate the second experiment case, i.e. the casting under travelling magnetic stirring (TMS) which is applied in the direction of natural convection to enhance the natural convection. Crystal fragmentation of columnar dendrites is assumed as the sole origin of equiaxed crystals. Through the analysis of the simulation results, deep understanding to the experimentally reported phenomena was achieved. In comparison to the first experiment case of pure natural convection condition, the TMS-enhanced convection provides a favorable condition for columnar-to-equiaxed transition (CET) by homogenizing the temperature distribution in the bulk liquid region, enhancing the fragmentation of the columnar secondary arms and the transport of the fragments to bulk liquid region. Contradicting with the previous knowledge, the TMS-enhanced convection in this experiment case does not enhance the global macrosegregation significantly. However, it strengthens the channel segregates.

1. Introduction

Series of solidification experiments were performed to investigate the formation of as-cast structure and macro-/meso-segregation in rectangular castings (100 × 60 × 10 mm^3) of Sn-10wt%Pb alloy under different convection conditions: 1) natural convection; 2) travelling magnetic stirring (TMS) applied in the same direction of natural convection to enhance the convection; 3) TMS in the reverse direction of natural convection; 4) TMS in alternative directions [1]. These four experiment cases were precisely controlled/monitored: two heat exchangers to control the heating/cooling rate on both lateral walls of the sample ingot; 50 thermal couples to monitor the temperature field during cooling/solidification; metallographic analysis for the as-cast structure and macrosegregation, etc. Previously, the first experiment case (under natural convection) was successfully simulated by the authors [2]. The as-cast structure and macrosegregation shown a satisfactory agreement with the experiment. The current study will simulate the second experiment, i.e. the case under the TMS which is used to enhance the natural convection. The TMS device is placed in the bottom of the sample [3-7]. The inducted Lorentz force acts in the melt region near the bottom surface of the sample and decreases exponentially in the direction away from the bottom surface.

A three phase mixed columnar-equiaxed solidification model, as developed and further extended by the authors [8-10], was used to investigate the effect of TMS on solidification process, especially on the formation of as-solidified structure and macrosegregation. The primary goal of this work is to further validate the numerical model for the ability to 'reproduce' the experiment under the TMS.

2. Model description

The mixed columnar-equiaxed solidification model [8] was introduced previously. Main features are listed as follows:

- Three phases (liquid, equiaxed and columnar) are considered. Their volume fractions, f_ℓ, f_e and f_c, sum up to 1.0. The liquid and equiaxed are treated as the moving phases, and their velocities are obtained by solving the corresponding Navier-Stokes equations. The columnar dendrites, growing from the mold wall, are treated as stationary.
- Ideal morphologies are assumed for the two solid phases: globular morphology for equiaxed and step-wise cylinders for columnar with constant primary dendritic arm spacing λ_1. Considering the drag force and other hydrodynamic interactions, a grain envelope is assigned to equiaxed dendritic crystal. The solid dendrite and inter-dendritic melt are included in this envelope. In this study, the volume ratio of solid dendrite to equiaxed grain envelope f_{si} is set as 0.5.
- Fragmentation of columnar dendrites is considered as the sole source for equiaxed grains. The mass transfer rate by fragmentation from columnar phase to equiaxed phase is calculated with the formula: $M_{ce} = -\gamma \cdot \vec{u}_\ell \cdot \nabla c_\ell \cdot \rho_e$. The coefficient γ is introduced to bridge the unknown correlation between the fragmentation-induced mass transfer rate and other factors contributing to the fragmentation [10].
- The columnar-to-equiaxed transition (CET) occurs when the volume fraction of equiaxed grain envelope reaches to the criterion ($f_e^{env} = f_e/f_{si} = 0.49$) at the columnar tip front.
- All the volume-averaged concentrations (c_ℓ, c_e, c_c) are calculated and the macrosegregation is represented by a segregation index: $c^{index} = 100(c_{mix} - c_0)/c_0$, where the c_{mix} and c_0 are mixture concentration and initial concentration, where $c_{mix} = (c_\ell \cdot f_\ell \cdot \rho_\ell + c_e \cdot f_e \cdot \rho_e + c_c \cdot f_c \cdot \rho_c)/(f_\ell \cdot \rho_\ell + f_e \cdot \rho_e + f_c \cdot \rho_c)$. Thermodynamic equilibrium is assumed at the liquid-solid interface. Thus, the concentration difference between equilibrium (c_ℓ^*) and melt (c_ℓ) works for the driving force for the solidification.
- Electromagnetic forces acting on the melt and equiaxed grains are: $\vec{F} = \vec{B} \times \vec{J}$. It is calculated with the ANSYS Maxwell software.

3. Benchmark configuration

The experiment setup was described by Hachani and co-authors [1, 11, 12]. The geometry of sample ingot (Sn-10 wt% Pb) is a quasi-two dimensional rectangular (100 × 60 × 10 mm^3). Two heat exchangers set at the two lateral walls were used to control the solidification unidirectionally (figure 1). The temperature difference between these two exchangers was 40 K, and the cooling rate was 0.03 K/s. Because the heat contact resistance exists between the heater and the two lateral walls, the temperature difference between these two side walls is much smaller, approximately 20 K [1, 13]. On each of two heat exchangers, 9 thermocouples were arranged to measure the heat flux extracted from the ingot. Except for these two narrow walls, all others were maintained adiabatic approximately. An array of 50 thermocouples fixed on the wide surface of the crucible by laser-welding was used to record the transient temperature field. Thermodynamic, thermal physical and other modeling parameters [2, 14] used in this study can be found in table 1.

A linear motor which generates the TMS was placed 5 mm underneath the bottom wall of the sample. The calculated electromagnetic force with the ANSYS Maxwell software is shown in figure 2. The inducted Lorentz force acts in the same direction of the thermo-solutal buoyancy to strengthen the melt convection and the motion of equiaxed phase along the sample bottom.

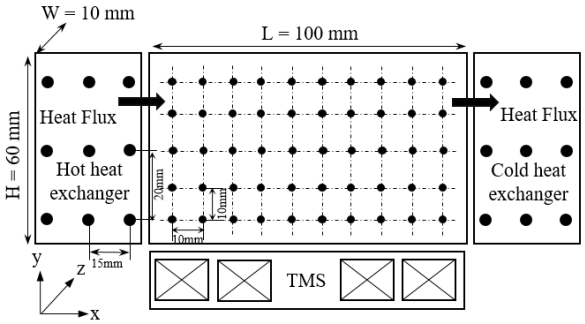

Figure 1. Sketch of the experiment setup: the location of the thermocouples (black dots), two heat exchangers, the travelling magnetic stirring.

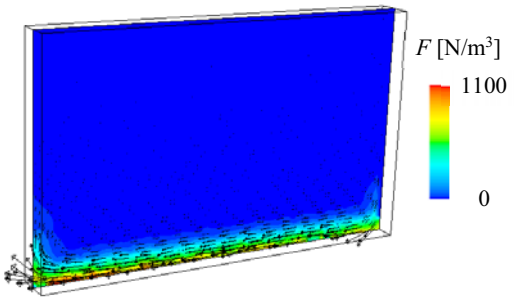

Figure 2. Distribution of electromagnetic force as shown in vectors and color scale.

Table 1. Thermo-physical properties of the alloy and other modeling parameters.

Property/parameters	Symbol	Units	Value
Nominal concentration of alloy (Pb)	c_0	wt%	10
Liquidus temperature	T_{liq}	K	492.46
Melting temperature of pure Sn	T_m	K	505.15
Partition coefficient	k_p	-	0.0656
Liquidus slope	m	K/(wt%)	-1.2826
Eutectic temperature	T_e	K	456.57
Eutectic concentration	C_e	wt%	38.1
Reference density	ρ_{ref}	kg/m^3	7000
Solid density	ρ_s	kg/m^3	7430
Thermal expansion coefficient	β_T	K^{-1}	6.0×10^{-5}
Solutal expansion coefficient	β_C	(wt%)$^{-1}$	-5.3×10^{-3}
Primary dendritic arm spacing	λ_1	m	2.25×10^{-4}
Secondary dendritic arm spacing	λ_2	m	6.5×10^{-5}
Diffusion coefficient in liquid	D_ℓ	m^2 s^{-1}	4.5×10^{-9}
Diffusion coefficient in solid	D_s	m^2 s^{-1}	1×10^{-12}
Latent heat	L	J/kg	6.1×10^4
Specific heat	c_{pl}, c_{ps},	J (kg K)$^{-1}$	260
Thermal conductivity	k_ℓ,k_e,k_c	W(m K)$^{-1}$	55
Viscosity	μ_ℓ	Pa s	1.0×10^{-3}
Gibbs-Thomson coefficient	Γ	m K	6.5×10^{-8}
Fragmentation coefficient	γ	-	0.5

4. Results

4.1 Solidification process

The calculated solidification sequence is shown in figure 3. A full 3D calculation was made, but here only the result on the middle vertical plane (z = 0.005 m) is presented. The starting point (t = 0 s) refers to the moment when the lowest temperature in the sample reaches the liquidus temperature.

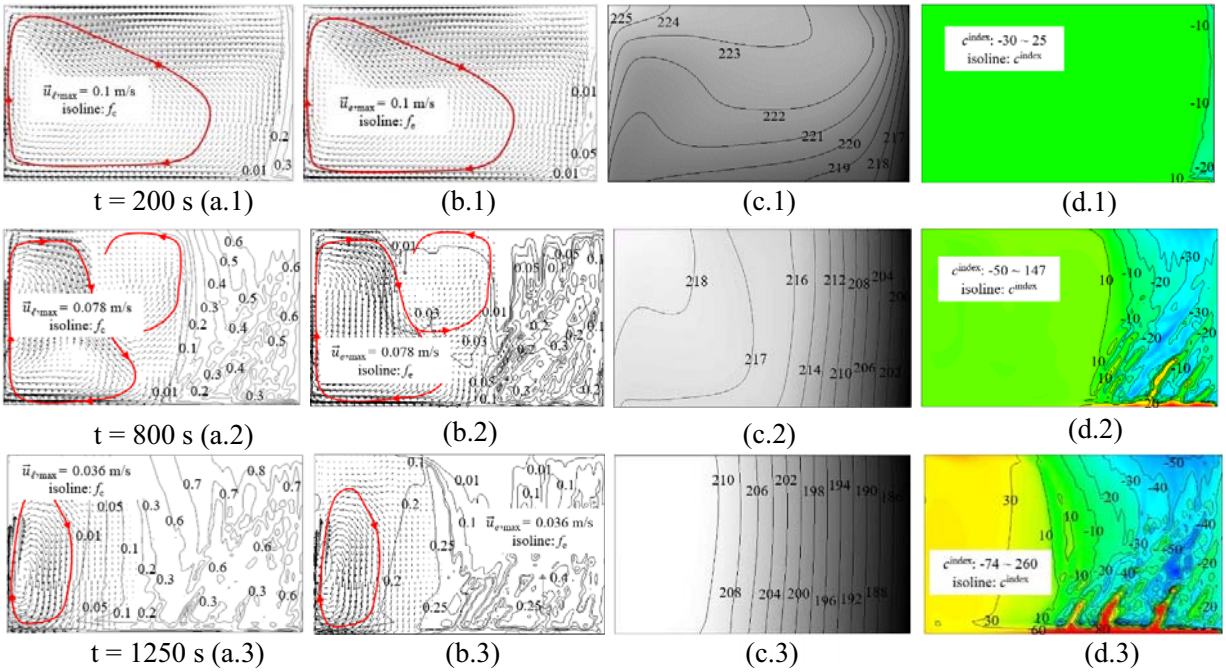

Figure 3. Solidification sequence of the casting sample (on the plane z = 0.005 m): (a.1 - a.3) liquid velocity overlaid with isolines of volume fraction of columnar phase, (b.1 - b.3) equiaxed velocity overlaid with isolines of volume fraction of equiaxed phase, (c.1 - c.3) temperature (°C) in grey scale and isolines, (d.1 - d.3) contour of the macrosegregation with the same c^{index} color scale (-80 ~ 80) and isolines, the real distribution range of c^{index} are labeled in the figures.

At the early stage of solidification (t = 200 s), due to the effect of thermo-solutal convection as enhanced by the TMS, a clockwise vortex biased towards the lower-left corner forms (figure 3(a.1)). The maximum velocities of liquid and equiaxed are equal to 0.1 m/s. As the superheat is extracted from the right side wall and the clockwise convection gathers the cold melt to the lower-right corner, the columnar dendrites initialize and grow from this region. Meanwhile, the equiaxed grains are produced by fragmentation mechanism in front of the columnar-liquid mushy zone (figure 3(b.1)). These heavier grains tend to sediment and also gather at the lower-right corner. Negative segregation starts to build up from the right-bottom corner; while the bulk region remains almost the initial concentration (figure 3(d.1)). The form of the isotherms can clearly show the effect of convection (figure 3(c.1)). The vortex caused by the TMS-enhanced convection makes a visible deformation of the isotherms.

At t = 800 s, the columnar dendrites continue to grow left-wards. Owing to the fact that the liquid density increases with the solute (Pb) enrichment and the increase in the number of equiaxed grains in the bulk region, the velocities of liquid and equiaxed decrease significantly. The maximum values of them are ca. 0.078 m/s (figure 3(a.2) - (b.2)). The TMS is still the dominant force to drive the melt flow and the motion of the equiaxed phase. To this moment, a new small vortex forms in the middle upper region. The newly formed equiaxed grains sediment and are brought into the left region. Additionally, the intensity of the melt flow is strong enough to bring some small grains upwards along the left wall. The equiaxed grains as located in the upper part grow and settle down again with the decrease of the temperature, further interact with the melt flow. The temperature field is also affected by this flow pattern (figure 3(c.2)). Channel segregates initialize and form in the columnar region. Negative segregation region extends leftwards. Correspondingly, positive segregation develops in the bulk melt region (figure 3(d.2)).

At t = 1250 s, the growth of the columnar primary dendrites tips is blocked by the accumulation of the equiaxed phase (figure 3(b.3)). Thus, the CET occurs ($f_e^{env} = f_e/f_{si} = 0.25/0.5 = 0.5 > 0.49$). The vortex is confined to the left part of rest liquid region, and the maximum velocities of liquid and equiaxed are gradually reduced to ca. 0.036 m/s. The isotherms are almost vertical in the solid region, while the temperature gradient almost disappears in the rest liquid region (figure 3(c.3)). More segregation channels form in the columnar region. Solute enriched melt gathers to promote more serious positive segregation in the rest liquid region (figure 3(d.3)).

4.2 As-cast structure

The simulated as-solidified structure, in comparison with the metallography of the experimental result is shown in figure 4. The global mixed columnar-equiaxed structure is well predicted by the simulation, i.e. the columnar structure occupies the right part, while the equiaxed region is mostly distributed in the left part (figure 4(c)). The isoline ($f_e^{env} = 0.49$) indicates the CET. The rest eutectic forms in the left-bottom corner, consistent with the experimental result as well (figure 4 - Zone1). However, some details of the as-cast structure can still not be modelled properly, e.g. the area of columnar phase in the upper region is overestimated by the simulation.

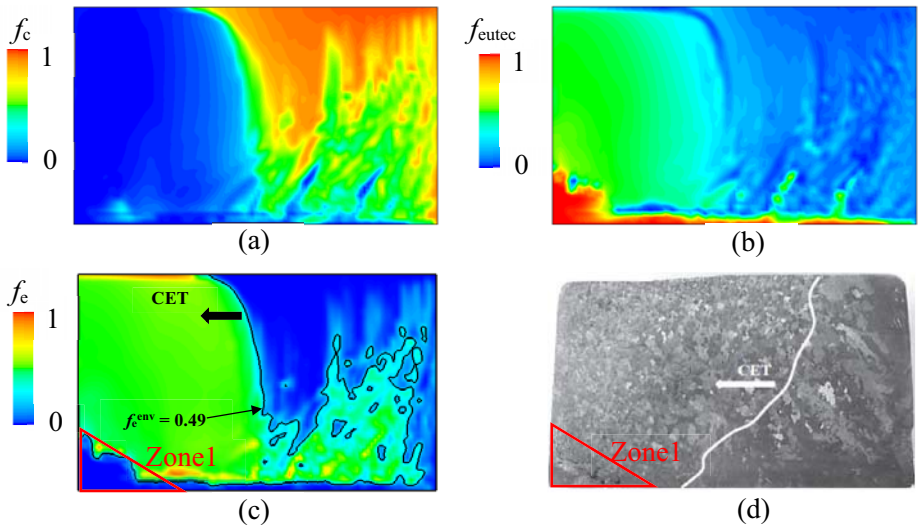

Figure 4. As solidified structure: (a) volume fraction of columnar, (b) volume fraction of the rest eutectic, (c) volume fraction of equiaxed phase overlaid with the isoline of $f_e^{env} = 0.49$, (d) metallographic analysis of the as-cast structure in the laboratory experiment.

4.3 Macrosegregation

The simulated macrosegregation map is compared with the X-radiography of the as-cast casting sample, as shown in figure 5. The X-radiography gives the macrosegregation information of the casting sample through the entire sample thickness, while the simulation result shows the c^{index} distribution on the vertical middle plane. This comparison shows a qualitative agreement between the simulation and the experiment. In the bright region of the lower-left corner, as shown by both simulation and experimental results, there is strong positive segregation; some segregation channels are found in the region of lower-right corner; negative segregation mostly occurs in the upper part.

Quantitative simulation-experiment comparison of the macrosegregation profiles along five horizontal lines (x-direction) were made in figure 6. Fifty measurement points were extracted from the as-cast sample. The positions of these points correspond to the thermocouple positions as shown in figure 1. The chemical

method coupled with inductive coupled plasma (ICP) technique were used to get the mean Pb concentration of each point. With this measurement method the channel segregates cannot be analyzed. In order to make a meaningful simulation-experiment comparison, the simulation results of c^{index} were also averaged along the sample thickness (z-direction). The figure 6 (a)-(e) correspond to the c^{index} profiles at y = 0.05, 0.04, 0.03, 0.02, 0.01 m (distance from the sample bottom). The experimental values and the simulation curves show very good agreement regarding to the segregation tendency. Generally, the simulation has overestimated the positive segregation in the left-side of the casting sample.

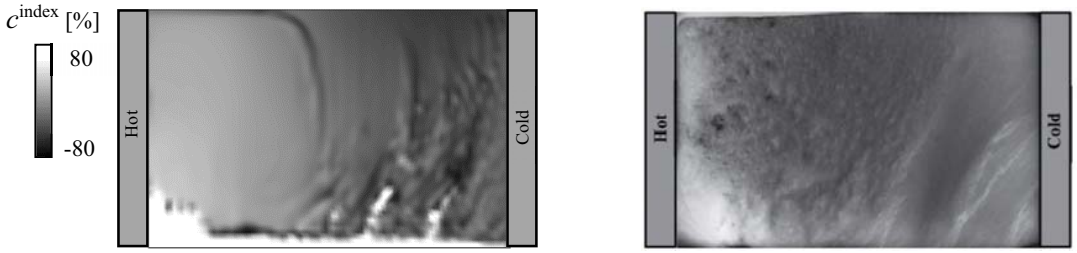

Figure 5. (a) Simulated macrosegregation distribution (c^{index}) on the vertical middle plane (z = 0.005 m), (b) X-radiography of the as-cast casting sample. The simulation result is shown in grey scale, with bright for positive segregation region and with dark for the negative segregation region.

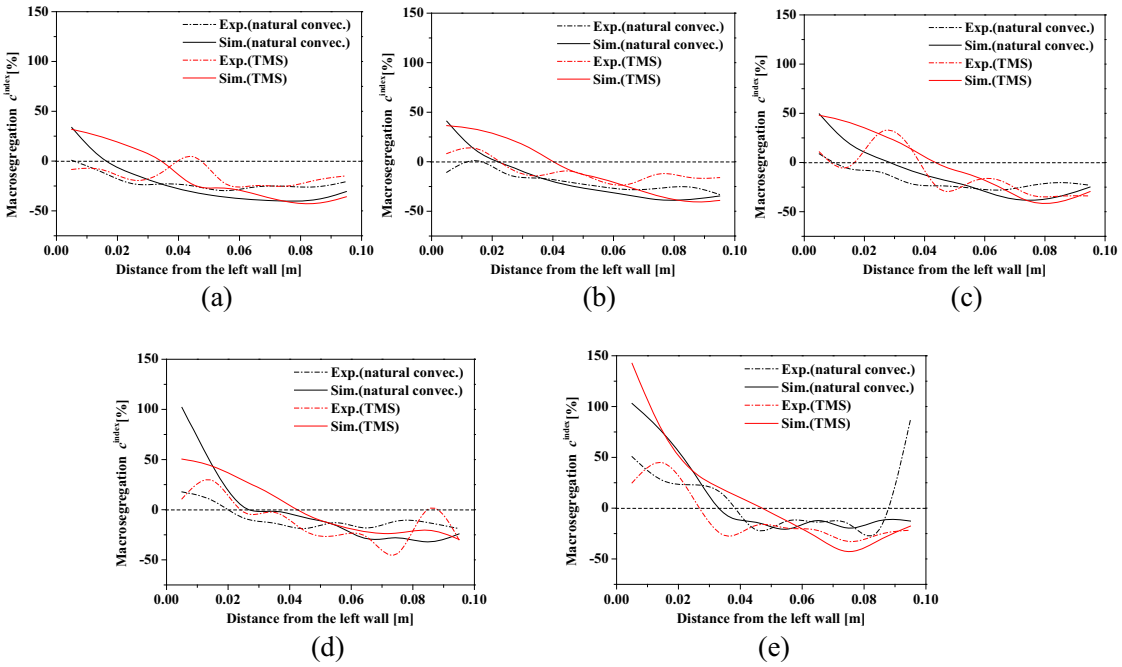

Figure 6. Comparison of the Pb-concentration between experimental analysis (black dotted line) and simulation (black solid line) along the horizontal lines: (a) - (e) correspond to the c^{index} profiles at y = 0.05, 0.04, 0.03, 0.02, 0.01 m (distance from the sample bottom). As reference (or comparison), the experimental analysis (red dotted line) and simulation (red solid line) for the experiment case of pure natural convection without applying TMS were also presented here.

5. Discussion

In this special experiment case, the TMS is applied in the bottom region of the casting sample and the inducted Lorentz force is used to intensify the thermo-solutal convection. In order to understand the effect of this TMS on the solidification process and the formation of as-cast structure and macrosegregation, the calculation for the case of pure natural convection is also made, and its result is compared with the calculation of the current case with TMS. The simulation settings of these two cases are identical except for the TMS. Figure 7 shows the calculated temperature distribution at time t = 900 s. For the case without TMS the temperature range in the sample is distributed between 221 °C (T_{max} = 494 K) and 193 °C (T_{min} = 466 K); while for the case with TMS the temperature range is between 218 °C (T_{max} = 491 K) and 199 °C (T_{min} = 472 K). It means the TMS-enhanced convection can homogenize the temperature field in the bulk liquid region effectively. This condition would favorite the growth of equiaxed structure. As-cast structure and macrosegregation between the two experiment cases are compared in figure 8. As shown in figure 8(b.1), a wider equiaxed zone forms for the case with TMS. The positive segregation zone, which corresponds to the last-to-solidified region, is more confined in the lower-left corner by the TMS-enhanced convection. Meanwhile, this forced convection seems to strengthen the channel segregates in the lower-right columnar region (figure 8(b.2)). However, contradicting to the general knowledge that stronger flow should result in more intensive macrosegregation, the TMS-enhanced convection in the current experimental condition does not strengthen the global macrosegregation significantly. This finding was also supported by the laboratory experiment as shown in figure 6, i.e. the experiment case with TMS did not show obvious stronger macrosegregation than that of the experiment case of pure thermo-solutal convection.

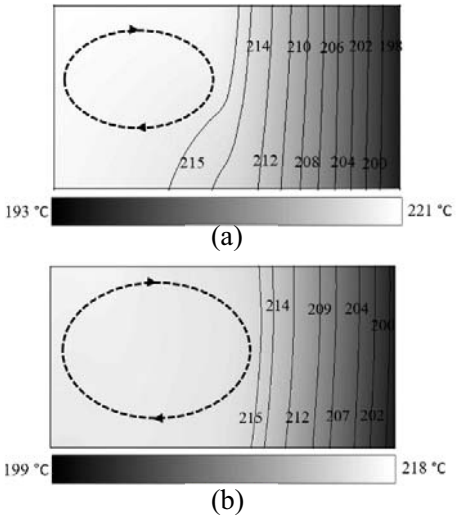

Figure 7. Temperature distribution of two different experiment cases (t = 900 s): (a) natural convection, (b) natural convection and TMS.

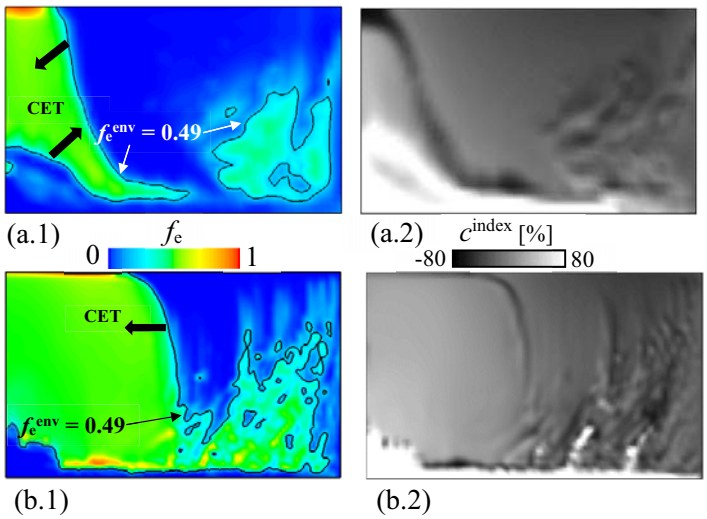

Figure 8. As-solidified structure (volume fraction of equiaxed overlaid with CET line) and macrosegregation (c^{index}) of two different experiment cases: (a.1-a.2) natural convection, (b.1-b.2) natural convection and TMS.

Although the distribution tendency of macrosegregation is well predicted by the numerical model, the quantitative difference between the simulation and experiment is still significant. As shown in figure 6, the positive segregation is overestimated. One main reason may be the ignorance of the remelting of the equiaxed crystals. During the late period of solidification, equiaxed crystals are brought by the flow from columnar tip front region into the bulk melt (left) region. Part of the crystals should have been re-melted there, and dilute the positive segregation to some extent in the lower-left corner region, but this remelting phenomenon is not considered. This model imperfection may be also responsible for some discrepancy

between the simulated as-solidified structure and experimental as-cast structure (figure 4). The second reason is the calculation of the travelling magnetic force (TMF). The design of the electromagnetic stirring device (necessary for the ANSYS Maxwell settings) has to be estimated due to lack of sufficient information. Additionally, most thermo-physical properties are not treated as temperature dependent, except for the buoyancy term in the momentum conservation equation where the density of the melt is considered as temperature and concentration dependent.

6. Conclusion

A mixed columnar-equiaxed solidification model was used to simulate the solidification of Sn-10wt%Pb alloy under forced convection condition driven by travelling magnetic stirring (TMS). The TMS is applied in the bottom region of the solidification sample, and the inducted Lorentz force acts to enhance the natural convection. The simulation result was compared with the experiment as performed by Hachani *et al.* [1]. The following conclusions were drawn.

(1) The simulation results agree qualitatively with the experimental results, regarding to the as-solidified mixed columnar-equiaxed structure and macrosegregation pattern. On this agreement, one can safely use the modeling results to analyze the complex solidification sequence, hence to achieve better understanding to the formation mechanisms of the as-cast structure and macrosegregation.

(2) In comparison with the experiment case of pure natural convection condition, the TMS-enhanced convection can create a favorable condition for CET by homogenizing the temperature field in the bulk liquid region, enhancing the fragmentation of the columnar secondary arms and the transport of these fragments to bulk liquid region. These fragments act as the origin of the equiaxed grains. Therefore, the TMS-enhanced convection leads to a wider equiaxed zone.

(3) In the current experiment case, the TMS-enhanced convection does not enhance the global macrosegregation significantly, but it strengthens the channel segregates.

Acknowledgments

The authors acknowledge the financial support from the Austrian Research Promotion Agency (FFG) through the project Bridge I (No. 868070).

7. References

[1] Hachani L, Zaidat K and Fautrelle Y 2015 *Int. J. Heat Mass Transf.* **85** 438-54
[2] Zheng Y, Wu M, Karimi-Sibaki E, Kharicha A and Ludwig A 2018 *Int. J. Heat Mass Transf.* **122** 939-53
[3] Avnaim MH, Mikhailovich B, Azulay A and Levy A 2018 *Int. J. Heat Fluid Flow* **69** 23-32
[4] Wang X, Fautrelle Y, Etay J and Moreau R 2009 *Metall. Mater. Trans. B* **40** 82
[5] Wang X, Moreau R, Etay J and Fautrelle Y 2009 *Metall. Mater. Trans. B* **40** 104-13
[6] Zaidat K, Sari I, Boumaaza A, Abdelhakem A, Hachani L and Fautrelle Y 2018 *IOP. Conf. Ser. Mater. Sci. Eng.* **424** 012052
[7] Yesilyurt S, Motakef S, Grugel R and Mazuruk K 2004 *J. Cryst. Growth* **263** 80-9
[8] Wu M and Ludwig A 2006 *Metall. Mater. Trans. A* **37** 1613-31
[9] Wu M, Ludwig A and Kharicha A 2019 *Metals* **9** 229
[10] Zheng Y, Wu M, Kharicha A and Ludwig A 2017 *Model. Simul. Mat. Sci. Eng.* **26** 015004
[11] Hachani L, Saadi B, Wang X, Nouri A, Zaidat K, Belgacem-Bouzida A, Ayouni-Derouiche L, Raimondi G and Fautrelle Y 2012 *Int. J. Heat Mass Transf.* **55** 1986-96
[12] Wang X and Fautrelle Y 2009 *Int. J. Heat Mass Transf.* **52** 5624-33
[13] Boussaa R, Hachani L, Budenkova O, Botton V, Henry D, Zaidat K, Hadid HB and Fautrelle Y 2016 *Int. J. Heat Mass Transf.* **100** 680-90
[14] Bellet M *et al.* 2009 *Int. J. Therm. Sci.* **48** 2013-6